Research Square

Preprints are preliminary reports that have not undergone peer review.
They should not be considered conclusive, used to inform clinical practice,
or referenced by the media as validated information.

Differential reflectance Signature of Fano Resonance and Antiresonance in a Reflective Au Diffraction-Grating Structure

Atsushi Motogaito

motogaito@elec.mie-u.ac.jp

Mie University

Keita Ukai

Mie University

Taiyo Nabuchi

Mie University

Takeshi Kato

Nagoya University

Kazumasa Hiramatsu

Mie University

Research Article

Keywords:

Posted Date: July 21st, 2026

DOI: https://doi.org/10.21203/rs.3.rs-10160367/v1

License: This work is licensed under a Creative Commons Attribution 4.0 International License.
Read Full License

Additional Declarations: No competing interests reported.

Version of Record: A version of this preprint was published at Applied Physics B on October 16th, 2026.
See the published version at https://doi.org/10.1007/s00340-026-08729-7.

Differential reflectance Signature of Fano Resonance and Antiresonance in a Reflective Au Diffraction-Grating Structure

Shortened version: Differential reflectance of Fano Resonance and Antiresonance

Atsushi Motogaito [1), *], Keita Ukai [1)], Taiyo Nabuchi [1)], Takeshi Kato [2, 3)], Kazumasa Hiramatsu [1)]

[1)] Graduate School of Engineering, Mie University, 1577 Kurimamachiya-cho, Tsu, Mie 514-8507, Japan

[2)] Institute of Materials and Systems for Sustainability, Nagoya University, Furo-cho, Chikusa-ku, Nagoya, Aichi 464-8603 Japan

[3)] Graduate School of Engineering, Nagoya University, Furo-cho, Chikusa-ku, Nagoya, Aichi 464-8603 Japan

*Corresponding Author: motogaito@elec.mie-u.ac.jp, ORCID: 0000-0002-7387-8469

Telephone number: +81-59-231-9399, Fax number: +81-59-231-9409

Abstract

We investigate the differential reflectance signature of Fano resonance and antiresonance in a reflective plasmonic grating structure. A double-layer Au diffraction grating—designed to operate in contact with ethanol under 780-nm illumination from the analyte side—is fabricated on a sapphire substrate using electron-beam lithography and vacuum deposition. Rigorous coupled-wave analysis reveals an asymmetric reflectance peak with steep angular variation, while numerical differentiation of the reflectance spectrum produces a sharp differential reflectance dip. Reflectance mapping combined with Rayleigh anomaly and propagating surface plasmon dispersion relations, along with electric-field distributions, indicates that the observed response originates from Fano-type coupling between localized surface plasmons at the grating edges and propagating surface plasmons at the Au/ethanol interface. Angular reflectance measurements reproduce both the asymmetric reflectance peak and differential reflectance dip, in good agreement with the simulations. The potential sensing performance is evaluated from the simulated refractive-index sensitivity and experimentally obtained linewidth. These results demonstrate that differential reflectance provides a useful readout of Fano resonance and antiresonance in reflective plasmonic grating sensors, particularly for low-refractive-index liquids.

1. Introduction

Surface plasmon resonance (SPR) sensors detect changes in the refractive index at metal–dielectric interfaces by monitoring plasmonic resonance conditions, enabling label-free and highly sensitive optical analysis of diverse analytes. SPR sensing has been widely applied in environmental monitoring, food safety, and biomedical diagnostics [1–3]. Among various SPR configurations—including prism-coupled [4--6], diffraction-grating [7--10], localized plasmon [11], and fiber-based sensors [12]—grating-coupled architectures are particularly attractive because they eliminate bulky prism optics and allow flexible control of resonance conditions, enabling more compact and integrable optical systems.

Conventional SPR sensors typically rely on tracking resonance peaks or dips in reflectance or transmittance spectra. However, the relatively broad linewidth of these features limits the figure of merit (FOM) and detection resolution, particularly for low-refractive-index liquids. Fano resonances—arising from the interference between a discrete state and a continuum [13]— provide an effective route to overcoming this limitation. They generate asymmetric spectral line shapes with sharp resonant peaks and antiresonant dips, leading to steep spectral or angular variations. In plasmonic nanostructures, such responses commonly result from interference between broad and narrow modes, including localized surface plasmons (LSPs), propagating surface plasmons (PSPs), and Rayleigh anomalies (RAs) [14--20]. In diffraction-grating systems, the interplay of these modes enables multiple resonant and nonresonant pathways, producing pronounced asymmetric reflectance features with enhanced sensitivity.

In our previous study, we demonstrated a SPR sensor based on a nonpropagating mode in a single-layer Au diffraction grating under normal-incidence transmission measurements [18]. Although initially interpreted as a nonpropagating surface-plasmon mode, the response was later understood as a Fano-type interaction between an edge-induced LSP and a PSP at the Au–medium interface. This work established the foundation of our plasmonic Fano sensor concept. However, the transmissive configuration is better suited to high-refractive-index media and is less effective for low-index liquid sensing.

For low-refractive-index liquids, a reflective configuration is more appropriate because it directly probes the plasmonic response at the metal–liquid interface from the analyte side. Moreover, the steep angular variation associated with Fano resonance and antiresonance can be further enhanced by analyzing the angular derivative of the reflectance, $\mathrm{d}R/\mathrm{d}\theta$. Near the transition between resonance and antiresonance, small changes in refractive index induce abrupt reflectance variations, resulting in a sharp dip in $\mathrm{d}R/\mathrm{d}\theta$. This feature provides a highly sensitive readout of the plasmonic response. The underlying mechanism can be understood in terms of phase-sensitive interference between resonant and nonresonant scattering channels, as described by temporal coupled-mode theory [15, 21]. While derivative-based interrogation has been explored in prism-coupled SPR systems, its application to reflective grating-based configurations exploiting Fano resonance for low-index sensing remains largely unexplored.

In this study, we design, fabricate, and characterize a reflective plasmonic Fano sensor based on a double-layer Au diffraction grating. We systematically investigate the relationship between asymmetric

reflectance, differential reflectance features, and Fano resonance/antiresonance behavior using rigorous coupled-wave analysis (RCWA), reflectance mapping, dispersion analysis, and electric-field distributions. The simulated results are experimentally verified through angular reflectance measurements in ethanol under 780 nm illumination. Finally, the potential sensing performance is estimated based on the refractive-index dependence and the experimentally obtained linewidth of the differential reflectance dip.

2. Structure, simulation, and experiment

2.1 RCWA Simulations

RCWA simulations were performed in MATLAB (MathWorks) using the open-source rcwa-2d package (SourceForge). Figure 1 illustrates the schematic of the simulated sensor structure, comprising a one-dimensional Au diffraction grating fabricated on a sapphire substrate and directly interfaced with the liquid analyte. The grating structure comprises a double-layer configuration of a 100 nm electron-beam resist and a 50 nm Au film with a 5 nm Cr adhesion layer. The grating period was fixed at 440 nm with a duty cycle of 50%. Ethanol (refractive index n = 1.36) was used as the surrounding medium, and optical responses were evaluated under 780 nm illumination incident from the analyte side. Angle-dependent transmittance and reflectance spectra were calculated for TM-polarized light. To further analyze the sensing mechanism, reflectance maps and electromagnetic field distributions were obtained from the RCWA simulations. The differential reflectance spectrum, $dR/d\theta$, was derived by numerically differentiating the angular reflectance spectrum.

2.2 Experimental methods

The structures shown in Figure 1 were fabricated on C-plane sapphire substrates using electron-beam lithography (EBL; JBX6300FS, JEOL) and vacuum deposition (VPC-260F, ULVAC). The term “double-layer structure” denotes a diffraction-grating structure consisting of an electron-beam resist relief pattern and a Cr/Au metal layer deposited on both the resist pattern and the exposed sapphire surface. Prior to fabrication, the substrates were cleaned with organic solvents and spin-coated with a ZEP-520A resist (Zeon). The resist was patterned using EBL and subsequently developed to form a periodic relief structure. A Cr/Au layer was then vacuum deposited over both the patterned resist and exposed substrate surface, resulting in a double layer diffraction grating. In this configuration, the resist pattern is retained as part of the final optical structure, eliminating the need for a lift-off process. Because the refractive indexes of the resist and sapphire substrate are similar, the developed resist pattern effectively defines the optical grating without requiring substrate etching. This lift-off-free fabrication approach using the electron-beam resist pattern as an optical structural layer was employed in our previous plasmonic grating and metasurface studies [22--26].

The fabricated structures were characterized using scanning electron microscopy (SEM) and atomic force microscopy (AFM) to confirm structural fidelity and surface morphology. The angular reflective

spectra were measured using a 780 nm laser source (PGL-780, Coherent). The sample—in contact with ethanol—was irradiated with p-polarized light from the analyte side. Reflectance spectra were obtained by measuring the reflected intensity as a function of incident angle. The differential reflectance spectrum was subsequently calculated from the measured data.

3. Simulated and differential reflectances

Figure 2 presents the angular spectra of transmittance, reflectance, and differential reflectance for ethanol, calculated using the RCWA method. The lower panel shows the transmittance and reflectance spectra, while the upper panel displays the differential reflectance spectrum. The reflectance spectrum exhibits a broad and asymmetric peak, gradually increasing from approximately 10.0° to 17.8°, followed by a sharp decrease beyond this angle. Such asymmetry is characteristic of Fano-type interference. However, the relatively large linewidth of the reflectance peak limits the achievable figure of merit when using conventional peak-tracking approaches. To address this limitation, the differential reflectance, dR/dθ, was evaluated by numerically differentiating the reflectance spectrum. As shown in the upper panel, this treatment reveals a pronounced and narrow dip near 17.8°, corresponding to the angular position of the maximum reflectance. This sharp differential feature originates from the steep angular variation of reflectance in the vicinity of the Fano resonance/antiresonance transition, and it provides a more sensitive metric for refractive index detection than the original reflectance spectrum.

4. Origin of Fano resonance and antiresonance

To elucidate the origins of the observed spectral features, a reflectance map was calculated, as shown in Figure 3(a). The enhanced reflectance region (green-yellow region) at 780 nm corresponds to the gradual rise observed in the angular reflectance spectrum (Figure 2). The differential reflectance dip appears at the boundary between regions of high-reflectance (yellow) and low-reflectance (blue) regions, indicating a rapid angular variation in reflectance. To further interpret these features, dispersion curves for RAs and PSPs at the Au/ethanol and Au/sapphire interfaces are superimposed on the map in Figure 3(b). These dispersion relations were calculated using conventional grating-coupling conditions [10, 19, 20], expressed as:

$$RA: \frac{\omega}{c}\sqrt{\varepsilon_d} + mK = k_0 \sin\theta \tag{1}$$

$$PSP: \frac{\omega}{c}\sqrt{\frac{\varepsilon_d \varepsilon_m}{\varepsilon_d + \varepsilon_m}} + mK = k_0 \sin\theta \tag{2}$$

where ω is the angular frequency of the incident light, c is the speed of light, ε_d and ε_m are the dielectric constants of the dielectric media (ethanol or sapphire) and Au, respectively, k_0 is the free-space wavenumber, θ is the incident angle, K is the grating wave vector, and m is the diffraction order (integer).

The reflectance enhancement (yellow region) is located between the RA and PSP dispersion curves, indicating that the enhanced reflectance originates from a Fano antiresonance arising from interference between the LSP modes associated with the grating structure and PSPs at the Au/ethanol interface [14, 15, 18--20, 27]. Meanwhile, the differential reflectance dip lies close to the RA dispersion curve, supporting its attribution to a Fano resonance condition.

To further clarify the underlying mechanism, electric field distributions were calculated at representative incident angles; Figures 4 (a) and (b) show the field distributions at incident angles of 17.8° and 17.4°, corresponding to the differential reflectance dip and the gradually increasing reflectance region, respectively. In Figure 4(a), strong coupling between the LSP localized at the grating edges and the PSP mode at the Au/ethanol interface is observed. The PSP exhibits a dominant electric field component normal to the interface (z-direction) and propagates along the grating (x-direction), indicating efficient mode coupling. This condition corresponds to Fano resonance, where constructive interference enhances the field interaction and produces a sharp spectral feature. In contrast, in Figure 4(b), the coupling between LSP and PSP is weaker, and the field localization is less pronounced. This regime corresponds to Fano antiresonance, where destructive interference suppresses coupling and results in the broader, asymmetric reflectance response. The time evolutions of the electric-field distributions at incident angles of 17.8° and 17.4° are provided in the Electronic Supplementary Material.

5. Fabrication and experimental verification

Figure 5 shows the fabricated double-layer diffraction-grating structure. The SEM image confirms the formation of a periodic Cr/Au grating, while the AFM image and line profile verify that the resist relief structure was successfully formed with the designed period and geometry. Moreover, the AFM line profile indicates that the resist width, space width, and resist relief height were 227, 212, and 142 nm, respectively.

To validate the simulations, angular reflectance measurements were carried out for the fabricated structure in contact with ethanol under 780 nm illumination. The measured reflectance and corresponding differential reflectance spectra are shown in Figure 6, where the lower panel represents the reflectance and the upper panel shows $dR/d\theta$. The experimental results reproduce the key features predicted by the simulations, including the asymmetric reflectance peak and a sharp differential reflectance dip near 17.5°. The slight angular shift from the simulated value can be attributed to fabrication tolerances and material-parameter variations. The relatively large noise in the differential reflectance spectrum is mainly attributed to the coarse angular sampling interval of 0.5° used in the reflectance measurement with a manual rotation stage. Because the differential reflectance is obtained from the angular derivative of the measured reflectance, fluctuations in the reflectance data are amplified when the angular interval is large. This noise is expected to be reduced by using a motorized rotation stage with finer angular resolution. Overall, the strong agreement between simulation and experiment confirms that the proposed reflective

plasmonic Fano sensor provides a sharp differential reflectance response in a low-refractive-index medium.

6. Potential sensing performance

To evaluate the potential sensing performance of the proposed structure, the refractive-index dependence of the differential reflectance dip was analyzed using RCWA simulations. Figure 7 shows the calculated reflectance and differential reflectance spectra for surrounding refractive indices in the 1.36–1.56 range. As the refractive index increases, both the reflectance peak and differential reflectance dip shift toward lower incident angles.

From the angular shift of the differential reflectance dip, the simulated angular sensitivity S_θ was estimated to be 49 deg/RIU. The FOM was evaluated using the standard linewidth-based definition for plasmonic refractive index sensors [2, 3, 16, 17, 28]:

$$FOM = \frac{S_\theta}{\Delta\theta_{\mathrm{FWHM}}} \tag{3}$$

where $\Delta\theta_{\mathrm{FWHM}}$ is the full width at half maximum of the differential reflectance dip. Using the simulated linewidth at n = 1.36, the simulated FOM was estimated to be 180 RIU^{-1}. In addition, a semi-experimental FOM of 41 RIU^{-1} was estimated by combining the simulated sensitivity with the experimentally measured linewidth of the differential reflectance dip.

The lower semi-experimental FOM is attributed to broadening of the differential reflectance dip in the experimental measurements compared to the simulations. This broadening likely arises from factors such as the finite angular resolution associated with the 0.5° sampling interval, alignment uncertainty, and measurement noise. Therefore, the reported FOM should be regarded as a semi-experimental estimate of the potential sensing performance. A more rigorous experimental evaluation, including direct sensitivity measurements using multiple liquids and a systematic analysis of the relationship between linewidth and angular resolution, will be addressed in future work.

7. Conclusion

We designed, fabricated, and characterized a lift-off-free reflective plasmonic Fano sensor based on a double-layer electron-beam resist/Au diffraction-grating on a sapphire substrate. RCWA simulations revealed a broad asymmetric reflectance peak and a sharp differential reflectance dip under 780 nm illumination in ethanol. Reflectance mapping and dispersion analysis showed that the reflectance enhancement occurs between the RA and PSP dispersion curves at the Au/ethanol interface, indicating a Fano antiresonance. In contrast, the sharp differential reflectance dip appears near the RA dispersion curve and corresponds to the Fano resonance condition. This interpretation is further supported by electric field distributions, which demonstrate strong coupling between LSPs at the grating edges and PSPs near the differential reflectance dip. Experimentally, the asymmetric reflectance peak and sharp differential

reflectance dip were observed at ~17.5°, in good agreement with the simulations. The simulated refractive-index dependence and experimentally obtained linewidth suggest the potential of the differential reflectance dip for refractive-index sensing. These results clarify the relationship between Fano resonance/antiresonance and the differential reflectance response in reflective plasmonic grating structures. The proposed approach offers a promising and practical readout strategy for compact SPR sensing of low-refractive-index liquids.

Disclosures and declarations

Acknowledgements

This work was supported by Grants in Aid for Scientific Research of the Japan Society for the Promotion of Science (JSPS, KAKENHI, Grant Nos. 23K04611 and 26K08228) and Advanced Infrastructure for Materials and Nanotechnology in Japan by the Ministry of Education, Culture, Sports, Science, and Technology, Japan (Grant Nos. JPMXP1224NU0209, JPMXP1225NU0206, and JPMX1226NU0206), Suzuki Foundation, and Takahashi Industrial and Economic Research Foundation. We extend our gratitude to Dr. Daiki Ohshima, Dr. Anna Honda, and Dr. Katsufumi Ohsumi from Nagoya University for their assistance with the electron-beam lithography system and atomic force microscopy. We would also like to thank Enago (www.enago.jp) for the English language review.

Funding

This work was supported by Grants in Aid for Scientific Research of the Japan Society for the Promotion of Science (JSPS, KAKENHI, Grant Nos. 23K04611 and 26K08228) and Advanced Infrastructure for Materials and Nanotechnology in Japan by the Ministry of Education, Culture, Sports, Science, and Technology, Japan (Grant Nos. JPMXP1224NU0209, JPMXP1225NU0206, and JPMX1226NU0206), IMaSS Joint Usage and Joint Research Program 2025 by The Institute of Materials and Systems for Sustainability, Nagoya University (Grant number 2025–1-042 and 2026-1-035), Suzuki Foundation, and Takahashi Industrial and Economic Research Foundation.

Competing interests

The authors have no relevant financial or non-financial interests to disclose.

Author contributions

Atsushi Motogaito and Kazumasa Hiramatsu contributed to the conception and design of the study. The simulation program was developed by Kazumasa Hiramatsu. The simulation was performed by Keita Ukai and Kazumasa Hiramatsu. Sample fabrication and SEM observation were performed by Keita Ukai and Atsushi Motogaito. Takeshi Kato provided instruction in electron beam lithography and performed AFM observations. Optical characterization was performed by Keita Ukai, Taiyo Nabuchi, and Atsushi Motogaito. All authors discussed the results of the simulation and experimental studies before and during the drafting of this manuscript. The first draft of the manuscript was written by Atsushi Motogaito, and all authors commented on all versions of the manuscript. All authors have read and approved the final manuscript.

Data availability statement

The datasets generated and/or analyzed during the current study are not publicly available due to potential intellectual property considerations but are available from the corresponding author upon reasonable request.

Ethics approval

This study does not require ethical approval.

Consent to participate

This study does not require voluntary informed consent to participate in the study.

Consent to publish

This manuscript does not contain any personal information.

References

1. Q. Duan, Y. Liu, S. Chang, H. Chen, J. H. Chen: Sensors 21, 5262 (2021)
2. V. Yesudasu, H. S. Pradhan, R. J. Pandya: Heliyon 7, e06321(2021)
3. J. Homola: Chem. Rev. 108, 462 (2008)
4. C. Nylander, B. Liedberg, T. Lind: Sens. Actuators 3,79 (1982)
5. E. Kretschmann: Z. Phys. 241, 313 (in German) (1971)
6. B. Liedberg, C. Nylander, I. Lunström: Sens. Actuators 4, 299 (1983)
7. H. Kano, S. Kawata: Jpn. J. Appl. Phys. 34, 331 (1995)
8. J. Homola, I. Koudela, S. S. Yee: Sens. Actuators B 54, 16 (1999)
9. J. Dostálek, J. Homola, M. Miler: Sens. Actuators B 107, 154 (2005)
10. A. Hessel, A. A. Oliner: Appl. Opt. 4, 1275 (1965)
11. K. R Ryu, G. W. Kim, J. W. Ha: Sci. Rep. 11, 12902 (2021)
12. Q. Wang, X. Z. Wang, H. Song, W. M. Zhao, J. Y. Jing: Opt. Laser Technol. 124, 106002 (2020)
13. U. Fano: Phys. Rev. 124, 1866 (1961)
14. B. Luk'yanchuk, N. I. Zheludev, S. A. Maier, N. J. Halas, P. Nordlander, H. Giessen, C. T. Chong: Nat. Mater. 9, 707 (2010)
15. A. E. Miroshnichenko, S. Flach, Y. S. Kivshar: Rev. Mod. Phys. 82, 2257 (2010)
16. G. Xiao, Y. Xu, H. Yang, Z. Ou, J. Chen, H. Li, X. Liu, L. Zeng, J. Li: Sensors 21, 1164 (2021)
17. R. Al Mahmud, R.H. Sagor, M.Z.M Khan: Opt. Laser Technol. 159, 108939 (2023)
18. A. Motogaito, A. Harada, K. Hiramatsu: Plasmonics 19, 2001 (2024)
19. F. Liu, X. Zhang, Biosens. Bioelectron 68, 719 (2015)
20. B. Stein, J.-Y. Laluet, E. Devaux, C. Genet, T. W. Ebbesen: J Phys. Chem C 116, 6092 (2012)
21. S. Fan, W Suh, J. D. Joannopoulos: J. Opt. Soc. Am. A 20, 569 (2003)
22. A. Motogaito, Y. Morishita, H. Miyake, K. Hiramatsu: Plasmonics 10, 1657 (2015)
23. A. Motogaito, T. Nakajima, H. Miyake, K. Hiramatsu: Appl. Phys. A 123, 729 (2017)
24. A. Motogaito, R. Tanaka, K. Hiramatsu: J. Eur. Opt. Soc.-RP 17, 6 (2021)
25. K. Akatsuka, K. Hiramatsu, A. Motogaito: Appl. Phys. B 130, 64 (2024)
26. A. Motogaito, R. Fukushi, Y. Takeshima, K. Ito, T. Kato, K. Hiramatsu: Opt. Rev. 33, 231 (2026)
27. V. G. Kravets, A. V. Kabashin, W. L. Barnes, A. N. Grigorenko: Chem. Rev. 118, 5912 (2018)
28. K. M. Byun, S. J. Kim, D. Kim: Appl. Opt. 46, 5703 (2007)

Figure caption

Fig. 1 Schematic of the reflective plasmonic Fano sensor based on a double-layer Au diffraction-grating structure

Fig. 2 Simulated angular spectra of transmittance, reflectance, and differential reflectance for the double-layer Au diffraction-grating structure in contact with ethanol

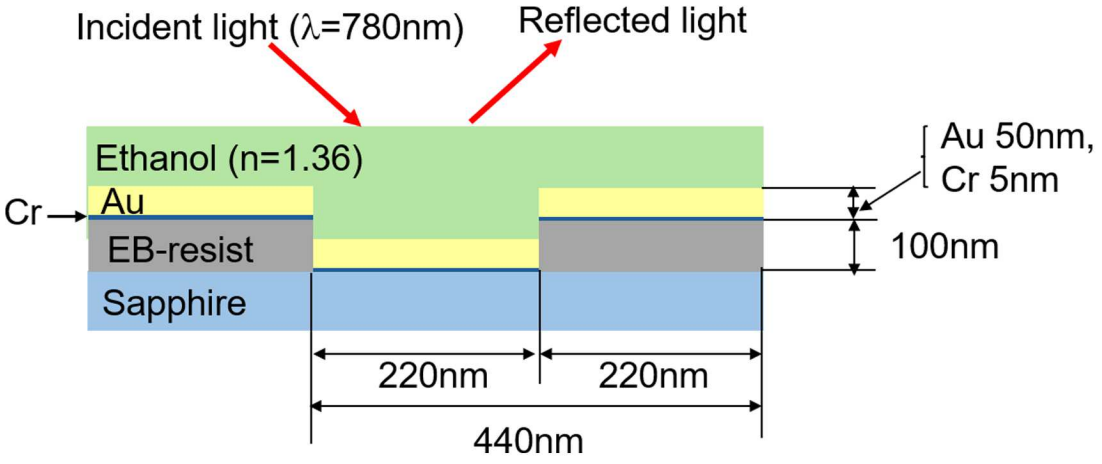
Fig. 3 Reflectance mapping calculated by rigorous coupled-wave analysis: (a) the reflectance map as a function of incident angle and wavelength; and (b) the reflectance map overlaid with the Rayleigh anomaly (RA) and propagating surface plasmon (PSP) dispersion curves at the Au/ethanol and Au/sapphire interfaces

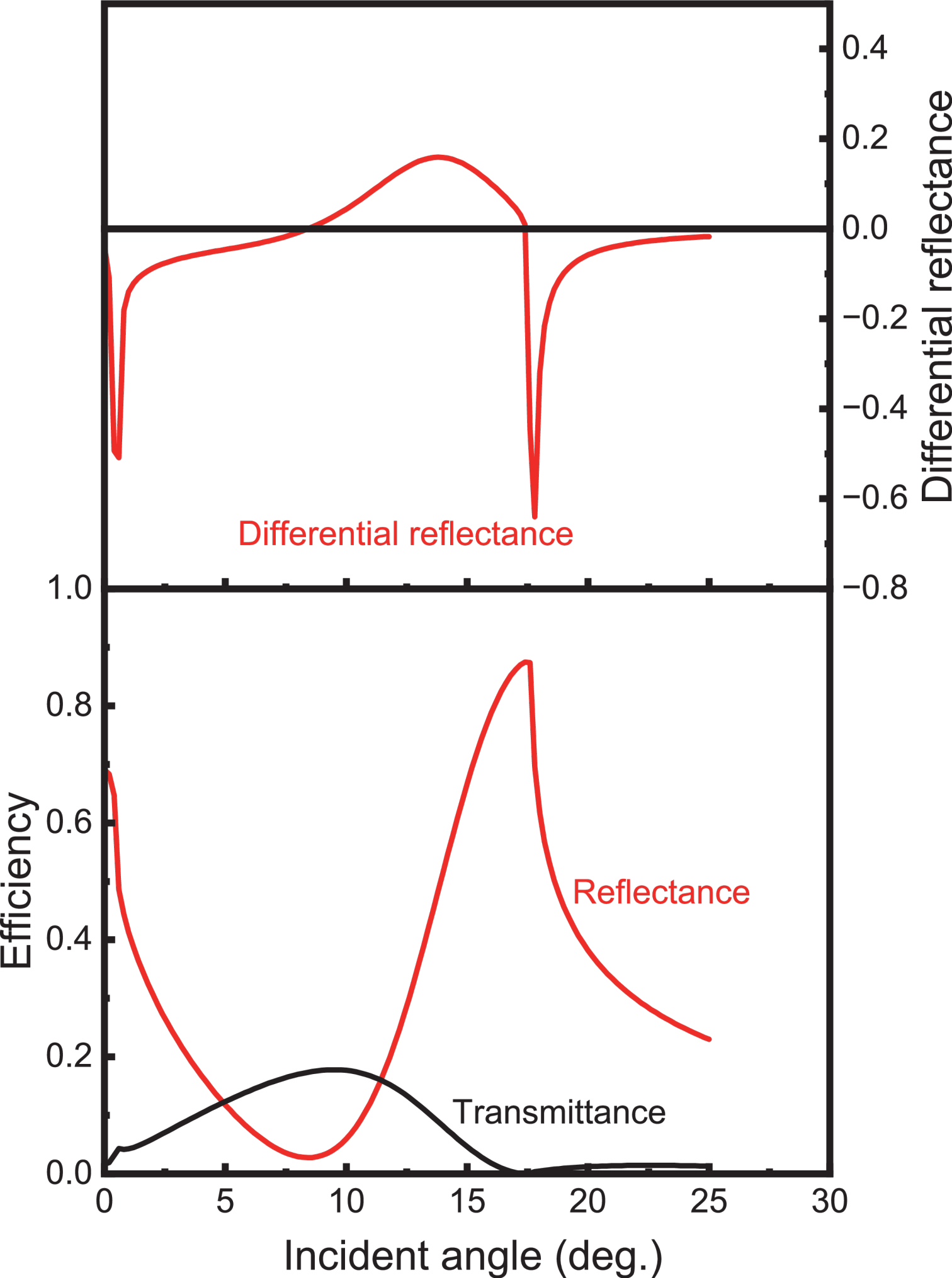
Fig. 4 Electric field distributions calculated by rigorous coupled-wave analysis at: (a) an incident angle of 17.8°, corresponding to the differential reflectance dip; and (b) an incident angle of 17.4°, corresponding to the gradual increase in reflectance

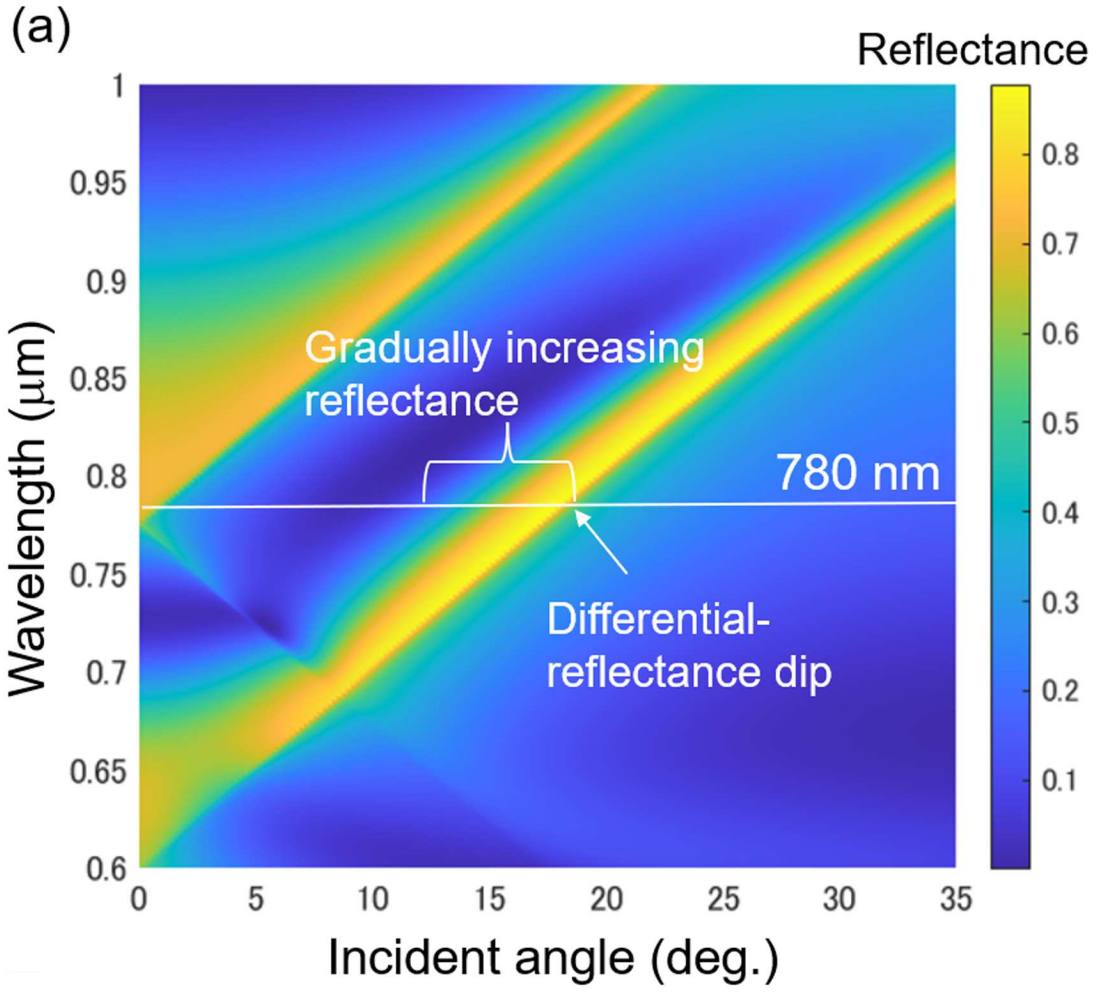
Fig. 5 Analysis of the fabricated double-layer diffraction-grating structure: (a) scanning electron microscopy image of the surface after Cr/Au deposition; (b) atomic force microscopy image of the electron-beam resist pattern before Cr/Au deposition; and (c) line profile of the resist pattern taken along the white line in (b). The red, green, and white triangles indicate the positions used to determine the resist width, space width, and resist relief height, respectively

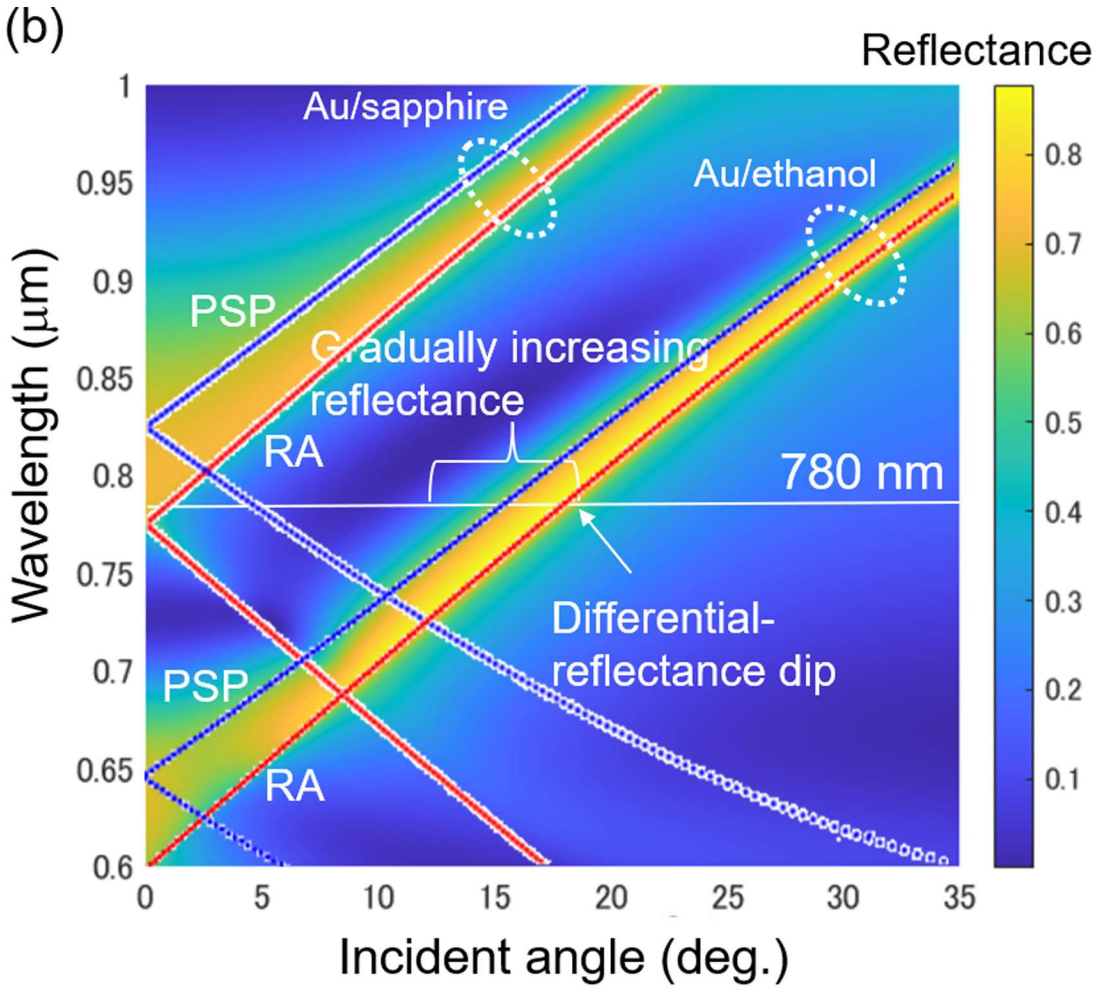
Fig. 6 Experimental and simulated angular spectra of the reflectance and differential reflectance measured in ethanol under 780 nm illumination

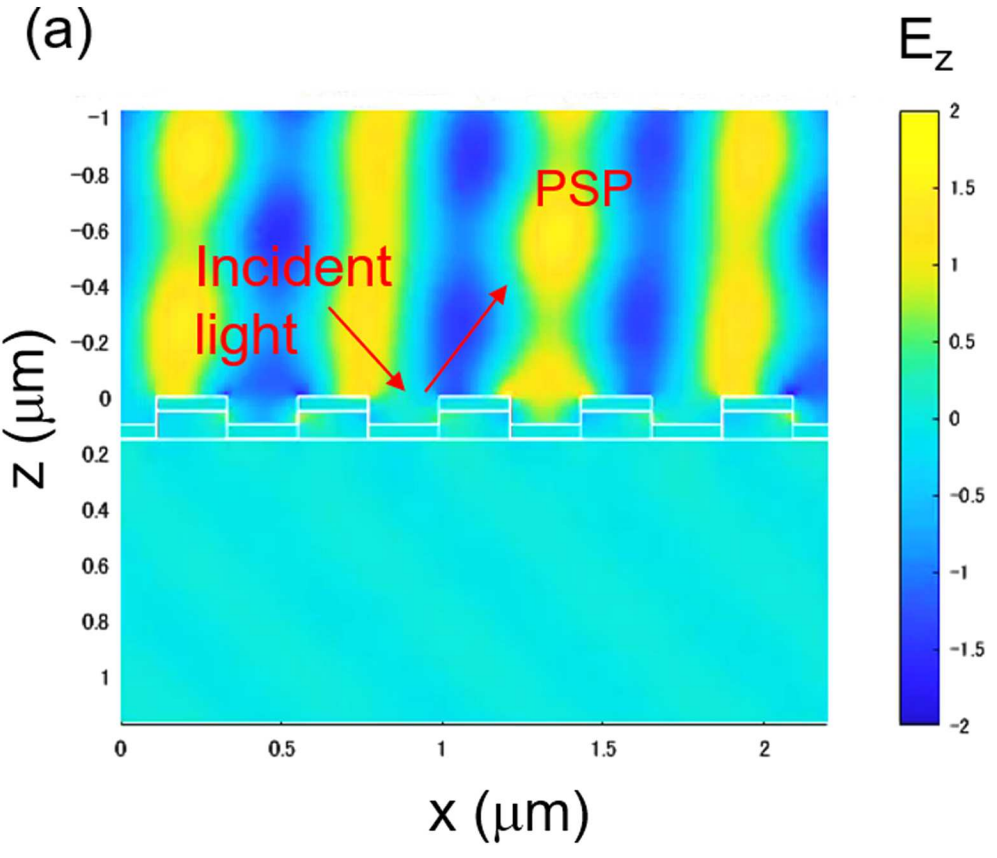
Fig. 7 Estimation of the potential sensing performance of the reflective plasmonic Fano sensor at refractive indices of 1.36 (red), 1.46 (blue), and 1.56 (black)

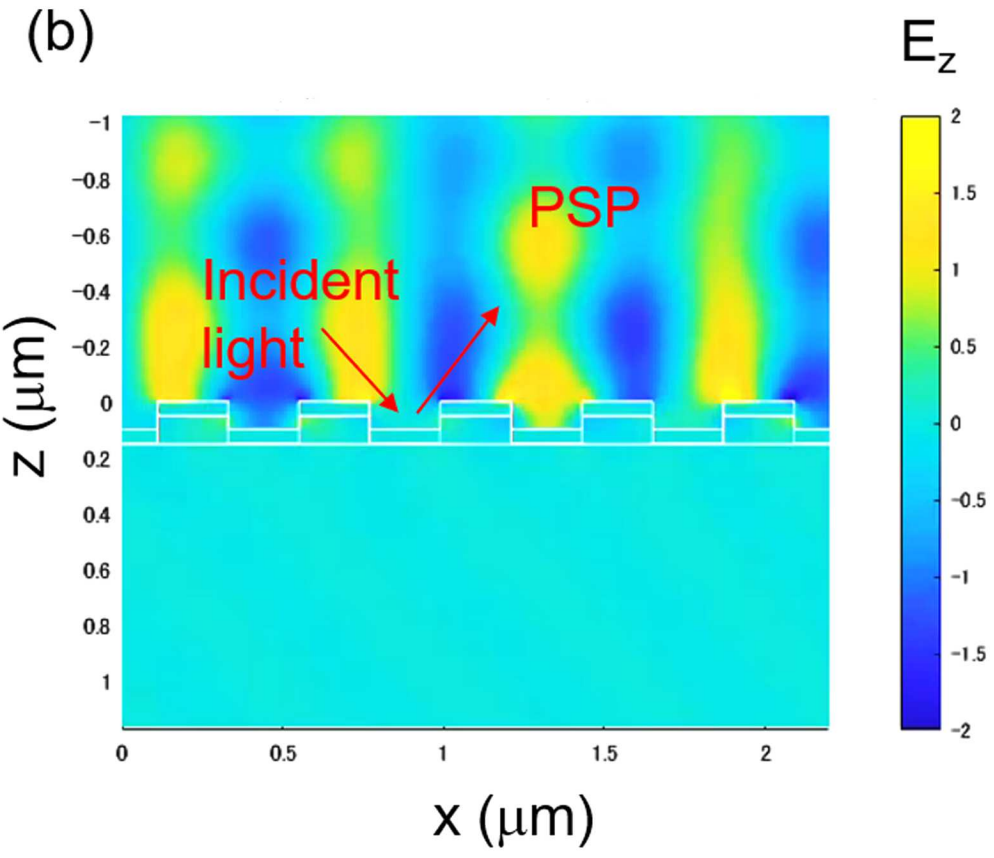

Incident light (λ=780nm)
Reflected light
Ethanol (n=1.36)
Cr
Au
EB-resist
Sapphire
Au 50nm,
Cr 5nm
100nm
220nm
220nm
440nm

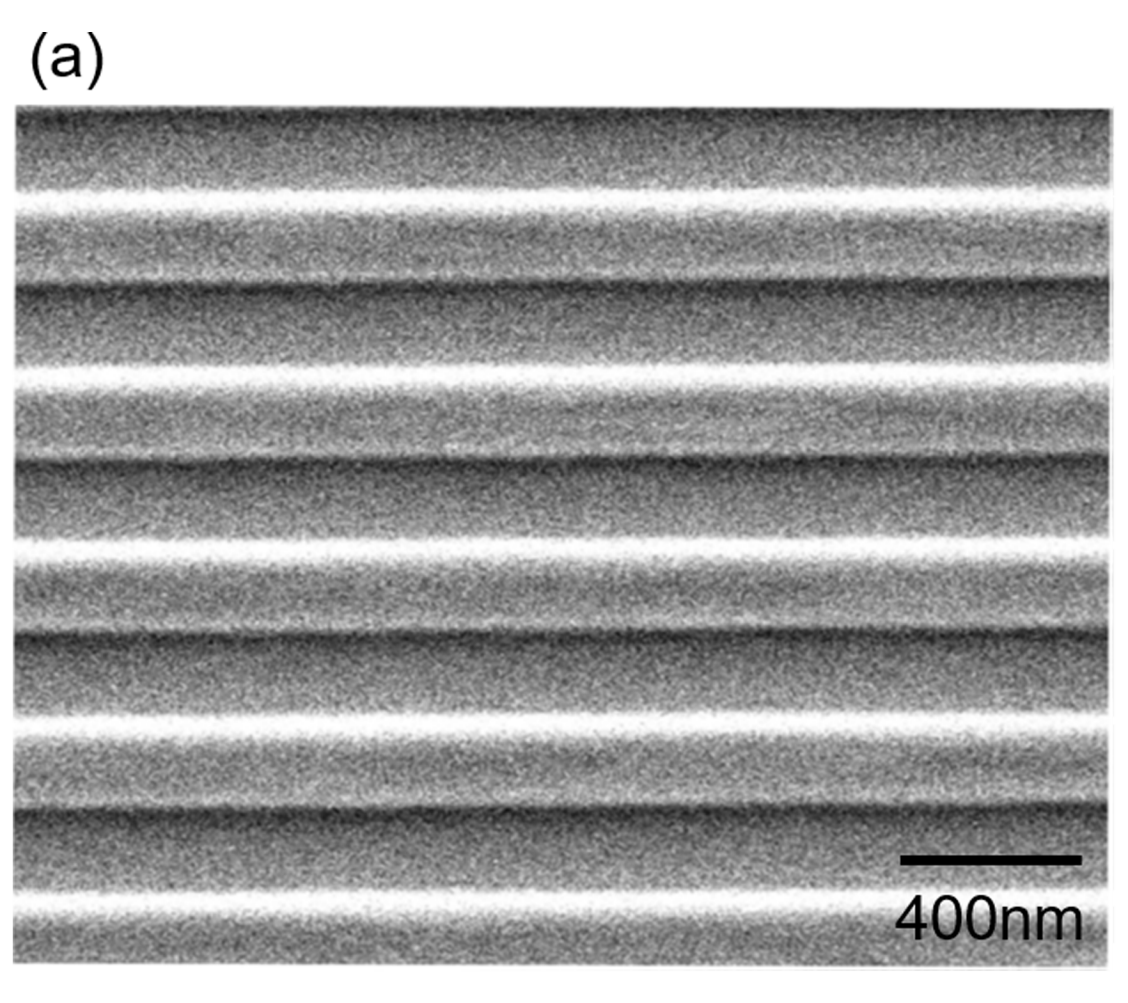

0.4
0.2
0.0
−0.2
−0.4
−0.6
−0.8
Differential reflectance
Differential reflectance
1.0
0.8
0.6
0.4
0.2
0.0
Efficiency
Reflectance
Transmittance
0
5
10
15
20
25
30
Incident angle (deg.)


(a)
Reflectance
1
0.95
0.9
0.85
0.8
0.75
0.7
0.65
0.6
Wavelength (μm)
0.8
0.7
0.6
0.5
0.4
0.3
0.2
0.1
Gradually increasing reflectance
780 nm
Differential-reflectance dip
0
5
10
15
20
25
30
35
Incident angle (deg.)

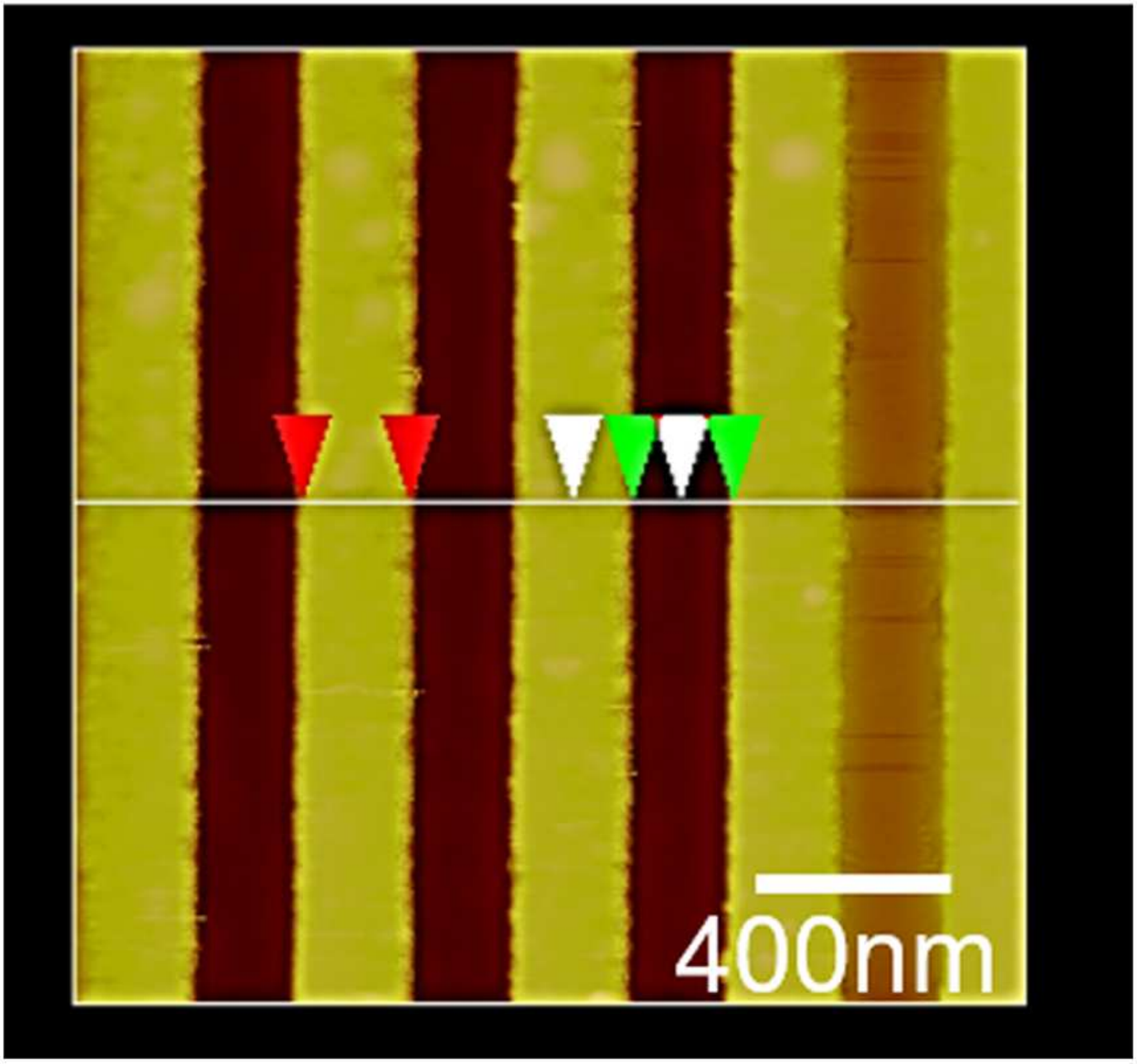

(b)
Reflectance
Au/sapphire
Au/ethanol
PSP
Gradually increasing reflectance
RA
780 nm
Differential-reflectance dip
PSP
RA
Wavelength (μm)
Incident angle (deg.)
1
0.95
0.9
0.85
0.8
0.75
0.7
0.65
0.6
0
5
10
15
20
25
30
35
0.8
0.7
0.6
0.5
0.4
0.3
0.2
0.1


(a)
E_z
PSP
Incident
light
z (μm)
x (μm)
−1
−0.8
−0.6
−0.4
−0.2
0
0.2
0.4
0.6
0.8
1
0
0.5
1
1.5
2
2
1.5
1
0.5
0
−0.5
−1
−1.5
−2

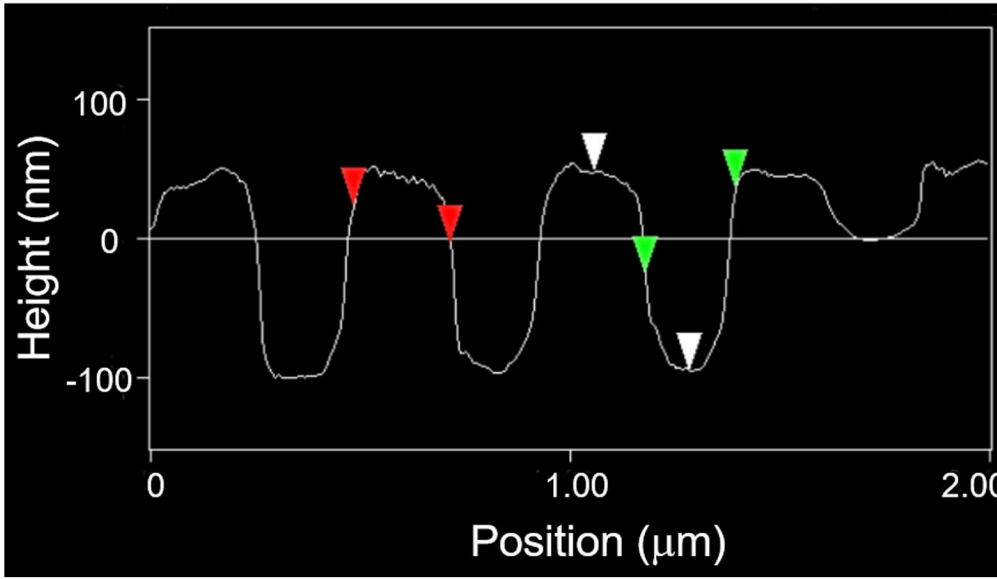

(b)
E_z
PSP
Incident
light
z (μm)
x (μm)
−1
−0.8
−0.6
−0.4
−0.2
0
0.2
0.4
0.6
0.8
1
0
0.5
1
1.5
2
2
1.5
1
0.5
0
−0.5
−1
−1.5
−2

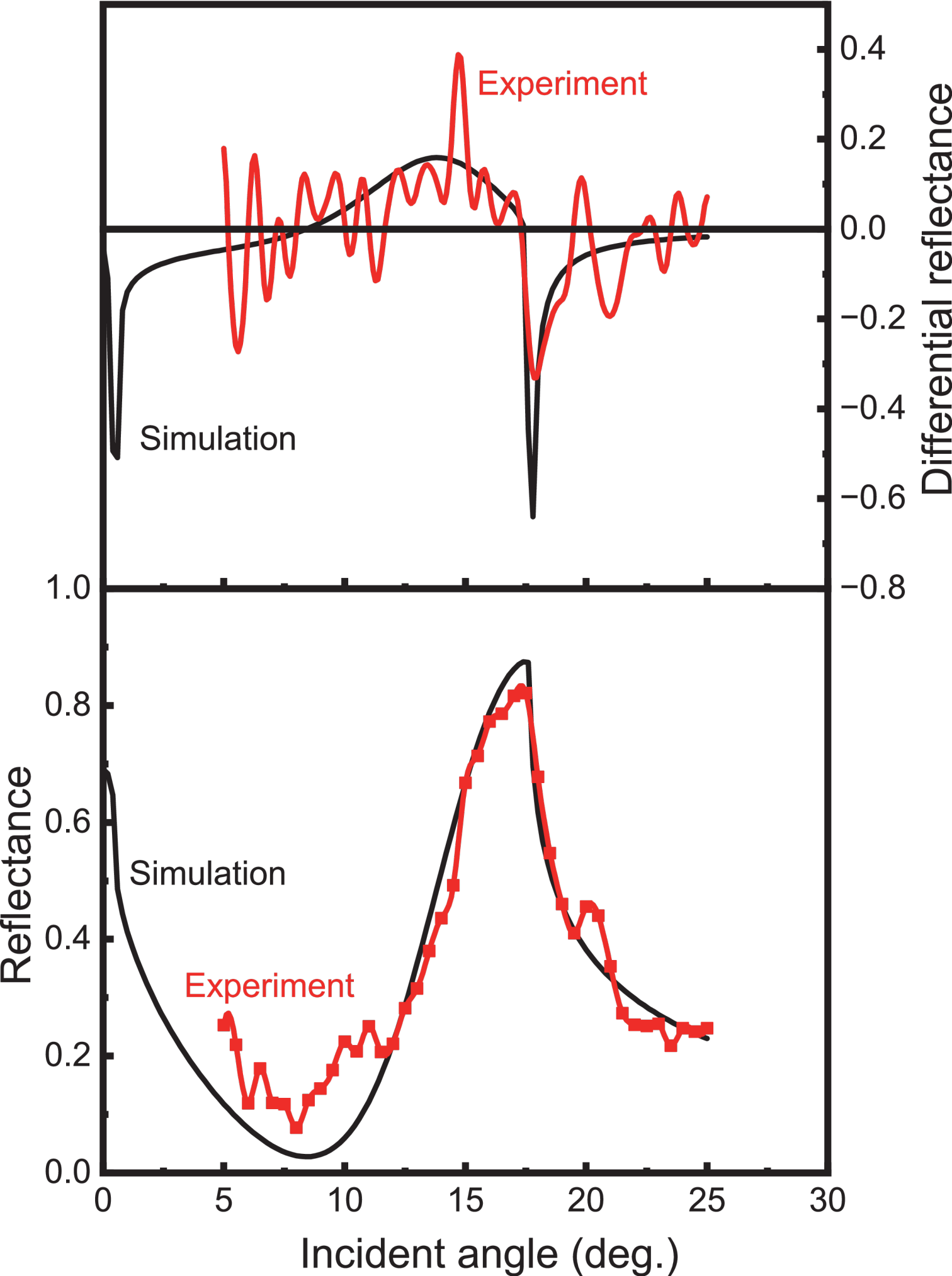

(a)
400nm

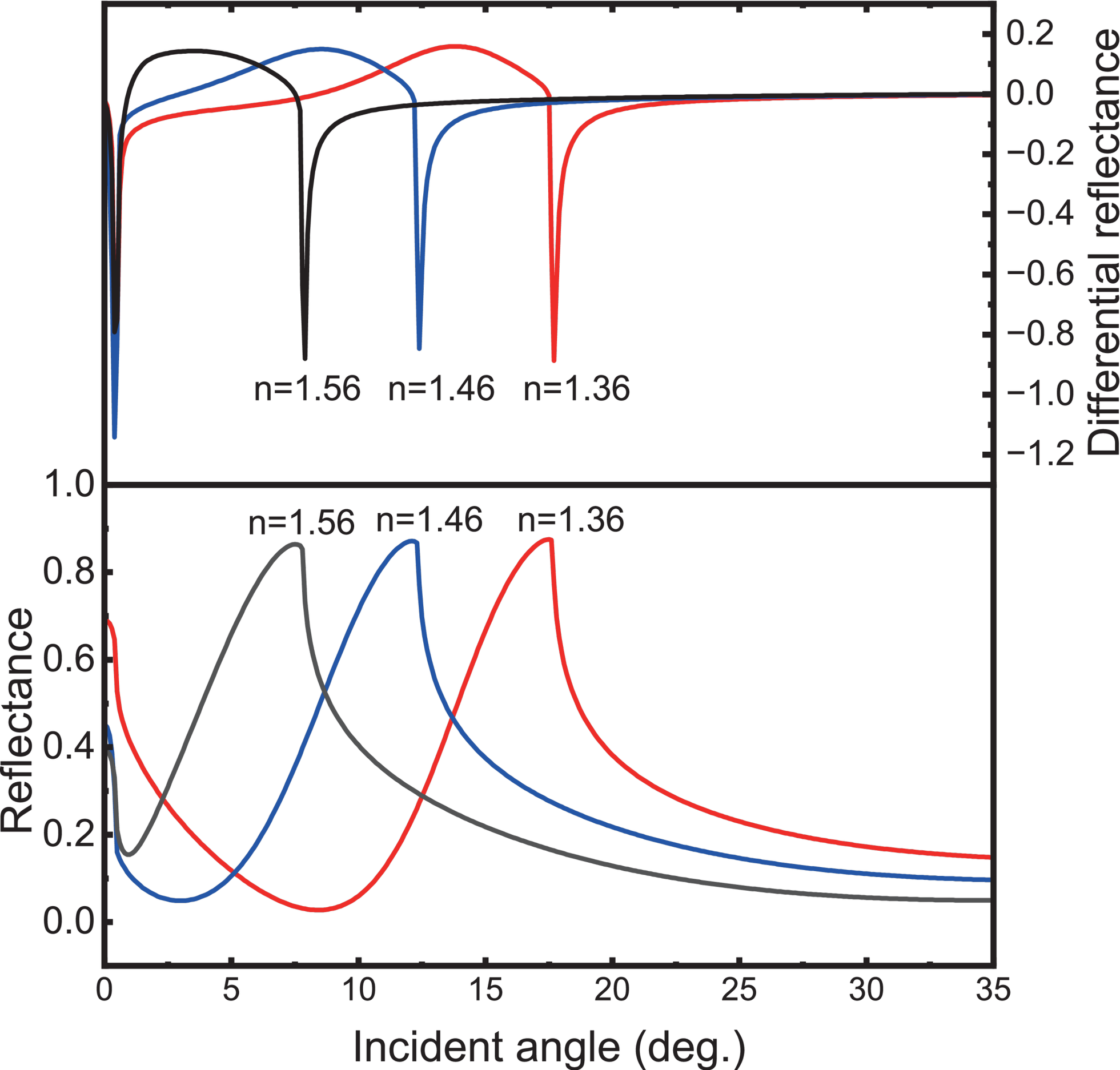
(b)



(c)




Experiment
Simulation
Differential reflectance
0.4
0.2
0.0
−0.2
−0.4
−0.6
−0.8
1.0
0.8
0.6
0.4
0.2
0.0
Reflectance
Simulation
Experiment
0
5
10
15
20
25
30
Incident angle (deg.)


0.2
0.0
−0.2
−0.4
−0.6
−0.8
−1.0
−1.2
Differential reflectance
n=1.56
n=1.46
n=1.36
1.0
0.8
0.6
0.4
0.2
0.0
Reflectance
n=1.56
n=1.46
n=1.36
0
5
10
15
20
25
30
35
Incident angle (deg.)

Supplementary Files

This is a list of supplementary files associated with this preprint. Click to download.

- Fig.4b.mp4
- Fig.4a.mp4